

## FIRST INTERSTELLAR HCO<sup>+</sup> MASER

NICHOLAS S. HAKOBIAN AND RICHARD M. CRUTCHER

University of Illinois at Urbana-Champaign, 1002 W. Green St. Urbana, IL 61801; *nhakobi2@illinois.edu, crutcher@illinois.edu*

*Accepted September 10, 2012*

### ABSTRACT

A previously unseen maser in the  $J = 1 - 0$  transition of HCO<sup>+</sup> has been detected by the Combined Array for Millimeter-wave Astronomy (CARMA). A sub-arcsecond map was produced of the 2 arcmin<sup>2</sup> region around DR21(OH), which has had previous detections of OH and methanol masers. This new object has remained undetected until now due to its extremely compact size. The object has a brightness temperature of  $> 2500$  K and a FWHM linewidth of  $0.497 \text{ km s}^{-1}$ , both of which suggest non-thermal line emission consistent with an unsaturated maser. This object coincides in position and velocity with the methanol maser named DR21(OH)-1 by Plambeck & Menten (1990). No compact HCO<sup>+</sup> emission was present in the CARMA data towards the other methanol masers described in that paper. These new results support the theory introduced in Plambeck & Menten (1990) that these masers likely arise from strong outflows interacting with low mass, high density pockets of molecular gas. This is further supported by recent observations of a CO outflow by Zapata et al. (2012) that traces the outflow edges and confirms that the maser position lies along the edge of the outflow where interaction with molecular tracers can occur.

*Keywords:* Astrochemistry – Masers – Molecular data – Stars: formation

### 1. INTRODUCTION

DR21(OH) is a part of a massive star forming region in the DR21 molecular cloud complex. It lies along a ridge of strong molecular emission extending from DR21 in the south to W75N in the north. As with many objects of its type, DR21(OH) also contains numerous sites of strong maser emission in many species. Named for its particularly strong OH-masers, it was determined that the OH and H<sub>2</sub>O masers were strongly coincident with millimeter continuum sources (Padin et al. 1989).

DR21(OH) is particularly significant due to the detection of methanol masers over a wide range of frequencies. Batrla & Menten (1988) detected methanol masers in the 81.6 GHz and 84 GHz methanol transitions. Plambeck & Menten (1990) conducted a study of 95 GHz methanol emission and found four strong methanol masers across a region associated with the MM2 millimeter source. Slysh et al. (1997) presented detections of a previously unseen 133 GHz methanol maser. More recently, Araya et al. (2009) present an extensive survey of over 30 44 GHz methanol masers, which appear to trace the shock fronts of two bow shocks along the red and blue shifted lobes of an outflow generated by MM2. Fish et al. (2011) present an analysis of all methanol maser detections and determine that all of the known masers appear to come from the interface region along the shock fronts of the outflow. The brightest of these masers appear along the western tip of the outflow and occur in a narrow velocity range of approximately  $0.3\text{-}0.5 \text{ km s}^{-1}$ . Additionally, they determine that all the methanol maser transitions are Class I masers, which arise from collisional excitations and are considered to be caused by shocks, especially those that arise from outflows, as opposed to Class II masers, in which the pumping mechanism is primarily derived from external radiation. Recent submillimeter continuum and 1 mm CO detections of the outflow morphology (Zapata et al. 2012) give further support to the above model. In this letter we report the first detection of an HCO<sup>+</sup> maser in the interstellar medium.

### 2. OBSERVATIONS

DR21(OH) was observed as part of an ongoing survey of sources (see Hakobian & Crutcher 2011) with strong mag-

netic field detections (Falgarone et al. 2008; Crutcher 1999). A 2 square arcminute region around DR21(OH) was mapped with observations by CARMA (Bock et al. 2006) in the C, D, and E array configurations with a combined effective beam size of  $6.3'' \times 4.0''$ , and a spectral resolution of  $0.41 \text{ km s}^{-1}$ . This was achieved by observing in the 8 MHz bandwidth correlator mode with 63 channels. The  $J = 1\text{-}0$  transition of HCO<sup>+</sup>, with a rest frequency of 89.188526 GHz, was simultaneously observed with HCN, N<sub>2</sub>H<sup>+</sup>, and two continuum bands. A bright, unresolved, and unusually narrow line feature was detected in the map of HCO<sup>+</sup> (Fig. 1), at  $20^{\text{h}}38^{\text{m}}59.3^{\text{s}} +42^{\circ}22'49.0''$  (J2000) with a peak at  $V_{\text{LSR}} = 0.78 \text{ km s}^{-1}$ . Each track was inspected to rule out the possibility of a transient instrumental issue; however, the compact source was visible in each track. The spatial and spectral location of the source additionally does not change between each of the tracks, indicating that an instrumental issue is unlikely. Follow-up observations in CARMA B-array configuration (Fig. 2) were performed in December 2011 in order to further constrain the physical size and brightness of the source. In total, five tracks of data were observed for a total of 18.75 hours: 4 hours each in B, C, and E arrays, and 6.75 hours in D array (over two tracks). Data were calibrated and imaged with the CARMA MIRIAD software package. The phase calibrator used in all tracks was 2038+513. Due to the strength of the calibrator, we were able to use the standard phase calibration techniques. The B-array track has an improved spectral resolution of  $0.14 \text{ km s}^{-1}$  over the other tracks, due to being observed with the expanded CARMA 8-band correlator in the 8 MHz bandwidth mode with 384 Hanning smoothed spectral channels (Figure 2 shows the 192 spectrally independent channels).

### 3. DATA / ANALYSIS

Using the high resolution B-array data, we find that the angular size of this object is less than  $\sim 0.8$  arcseconds and that it has a brightness temperature  $> 1900$  K. Since the source remained unresolved in B-array, the parameters of this object can be further constrained by using only long baseline components of the data set. This effectively “resolves out” larger scale structure, leaving a constrained map behind. To achieve this, we limited the map to use baselines larger than  $140 \text{ k}\lambda$

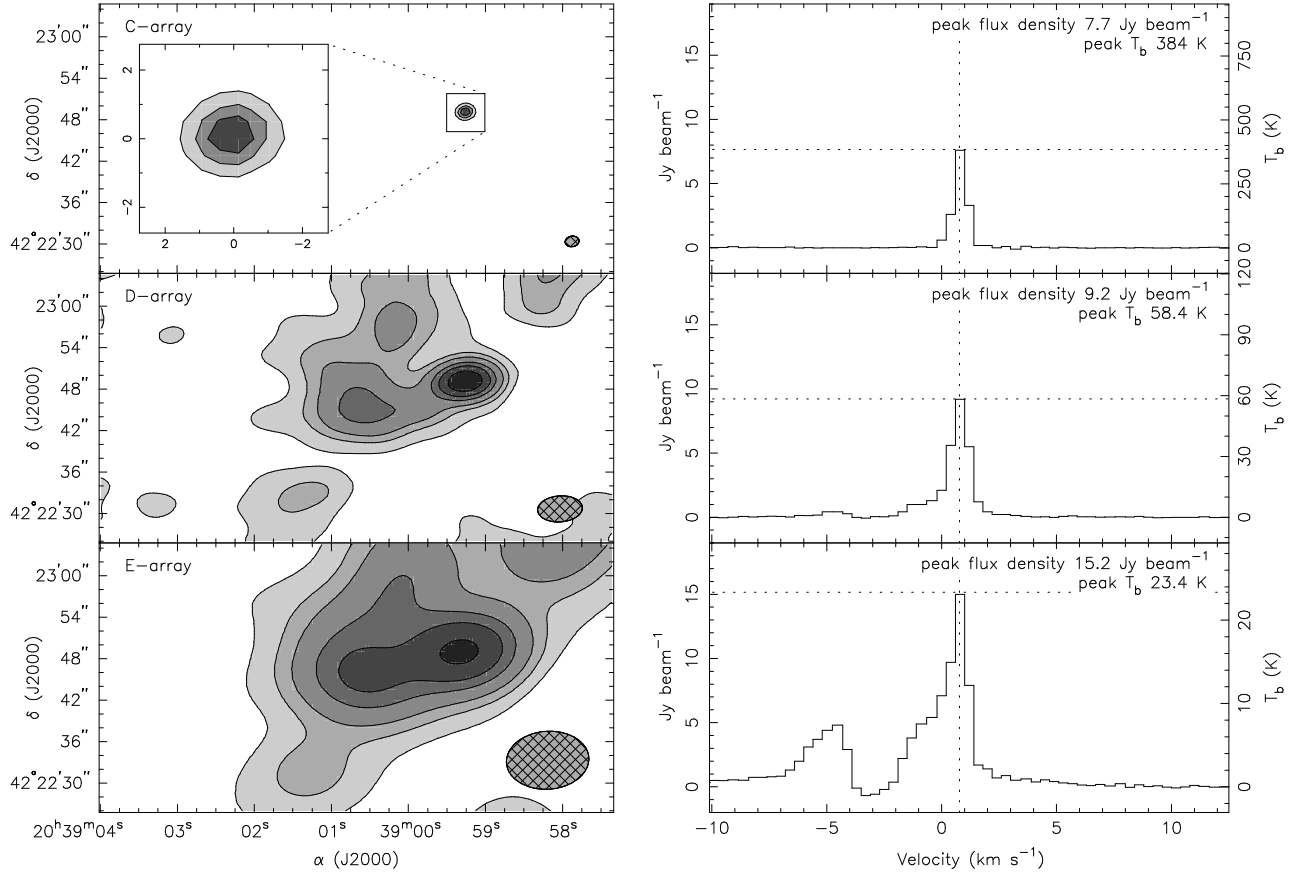


**Figure 1.** Comparison of maser emission in CARMA C, D, and E-arrays. Spectra (right) are of the peak positions in each map (left) of the  $0.78 \text{ km s}^{-1}$  channel, visible in shaded contours. The y-axis of the spectra are shown in both units of Flux density ( $\text{Jy beam}^{-1}$ ) and Brightness Temperature (K) to emphasize the effect of the decreasing source/beam size. The beam sizes are  $2.0'' \times 1.5''$ ,  $6.4'' \times 3.7''$ , and  $11.9'' \times 8.4''$  for the C, D, and E-array maps, respectively. The contour levels for the C-array map are 0.25, 0.50, and 0.75 times the peak flux density. The contour levels for the D and E-array maps are 0.01, 0.075, 0.15, 0.30, 0.45, and 0.7 times the peak flux density. The RMS noise of the spectra are 0.042, 0.028, and  $0.056 \text{ Jy beam}^{-1}$  for the C, D, and E array maps, respectively.

( $\sim 470$  meters). This procedure resulted in a map with an effective beam size of  $\sim 0.54'' \times 0.52''$  and a brightness temperature of  $> 2500 \text{ K}$ . The source appears to be unresolved even at this resolution (Fig 2, top panel).

If the source were dominated by thermal emission, a lower bound on its linewidth can be estimated by calculating the degree by which the emission would be thermally broadened. The calculated full-width at half maximum (FWHM) linewidth would then be purely a function of the effective brightness temperature:

$$\begin{aligned} \Delta f &= \sqrt{\frac{8kT \ln 2}{mc^2}} f_0, \quad \frac{\Delta f}{f_0} = \frac{\Delta v}{c}, \quad m = Nm_p \\ \Delta v &= \sqrt{\frac{8 \ln 2 k}{m_p}} \sqrt{\frac{T}{N}} \\ &= 0.2139 \sqrt{\frac{T}{N}} \text{ km s}^{-1} \end{aligned} \quad (1)$$

where  $T$  is the brightness temperature of the source and  $N$  is the atomic weight of the molecule. The factor of  $2\sqrt{2 \ln 2}$  comes from the conversion of a Gaussian standard deviation to FWHM. For a source with a brightness temperature of  $2546 \text{ K}$  and RMS noise of  $8.6 \text{ K}$  ( $0.015 \text{ Jy beam}^{-1}$ ), the thermal linewidth would be  $2.077 \pm 0.004 \text{ km s}^{-1}$ , which is significantly greater than the observed linewidth of  $0.497 \pm 0.002$

$\text{km s}^{-1}$  (obtained by least-squares gaussian fitting to the line profile). The maser linewidth corrected for the instrumental smoothing is  $0.477 \pm 0.002 \text{ km s}^{-1}$ . The observed high brightness temperature and linewidth narrowing are good indicators that this object is dominated by non-thermal emission. An assumption as to the type of maser emission can be made from this linewidth analysis. Saturated masers can have linewidths up to the thermal linewidth, while unsaturated masers will have a linewidth narrower than the thermal linewidth by a factor of 4 to 5 (Reid & Moran 1988). Since our object has a linewidth that is 4.2 times narrower than the thermal linewidth, it is consistent with an unsaturated maser.

Plambeck & Menten (1990) observed this region with BIMA at the  $95 \text{ GHz}$  methanol line and discovered four methanol masers connected by large scale methanol emission. The brightest of these four sources, DR21(OH)-1, is centered at  $20^{\text{h}}38^{\text{m}}59.24^{\text{s}} + 42^{\circ}22'49.04''$  (J2000) with a peak at  $V_{\text{LSR}} = 0.32 \text{ km s}^{-1}$ , which is approximately  $0.1''$  from the center of our measured  $\text{HCO}^+$  peak. The  $\text{HCO}^+$  position has an approximate positional error of  $0.2''$ , and the methanol positions have an error of  $0.3''$ . From these data they estimated their methanol maser had an angular diameter  $< 4.4''$  and a brightness temperature  $> 760 \text{ K}$ . Three other methanol masers were also observed; however, there is no evidence of companion  $\text{HCO}^+$  masers (Fig. 3). This could possibly be due to their relatively weaker strength or due to the fact that the condi-

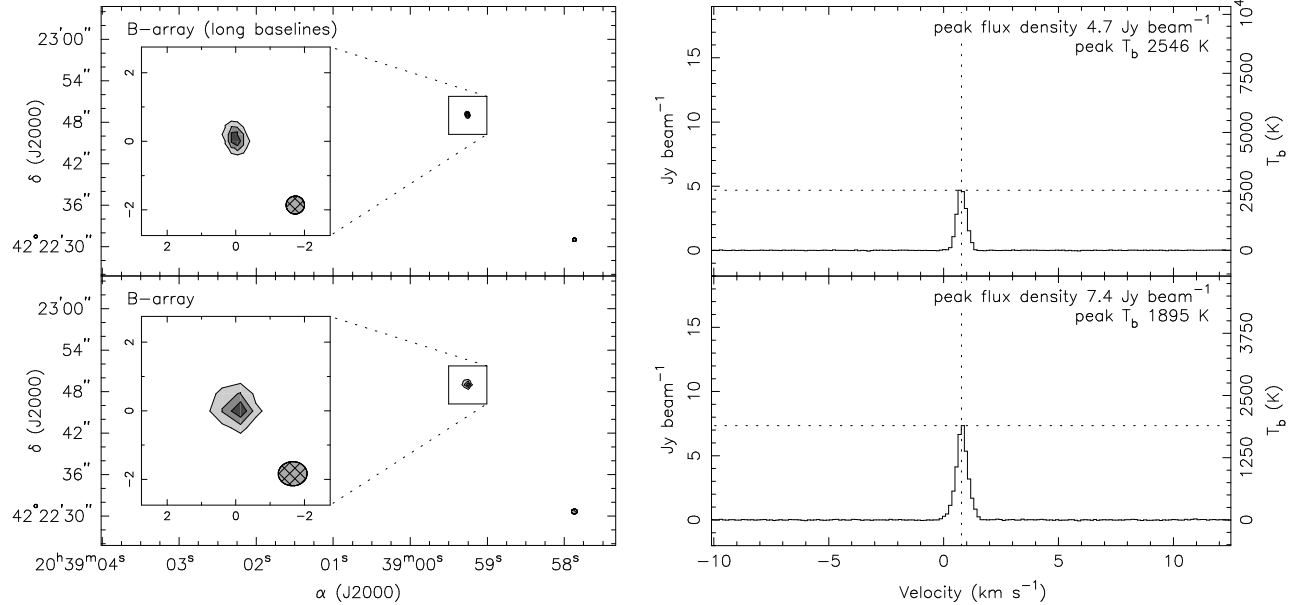


**Figure 2.** Comparison of maser emission in CARMA B-array. Spectra (right) are of the peak positions in each map (left) of the  $0.78 \text{ km s}^{-1}$  channel, visible in shaded contours. The y-axis of the spectra are shown in both units of Flux density ( $\text{Jy beam}^{-1}$ ) and Brightness Temperature (K) to emphasize the effect of the decreasing source/beam size. The maps feature an inlay showing the 4 arcsecond<sup>2</sup> region around the maser due to its compact size. The top panel is of B-array data with baselines  $> 140\lambda$ . The beam sizes are  $0.54'' \times 0.52''$  for the top panel, and  $0.85'' \times 0.70''$  for the bottom panel. The contour levels are 0.25, 0.50, and 0.75 times the peak flux density. The RMS noise of the spectra are 0.015 and 0.026  $\text{Jy beam}^{-1}$ , for the top and bottom map, respectively.

tions necessary to produce an HCO<sup>+</sup> maser do not exist at these other positions. The co-location of the HCO<sup>+</sup> object and the methanol maser suggest that both arise from similar conditions. Plambeck & Menten (1990) hypothesized that such regions could be created from the interaction of an outflow and small clumps of dense molecular gas.

In comparing the B-array maps (Figure 2), it appears as if the maser could be partially resolved since its intensity drops from  $7.4 \text{ Jy beam}^{-1}$  to  $4.7 \text{ Jy beam}^{-1}$  between them, with slight N-S structure. Araya et al. (2009) reports that there are three methanol masers within  $2''$  of the HCO<sup>+</sup> emission; one strong and two weaker masers, slightly north and south of the strongest maser. If the HCO<sup>+</sup> maser is also a complex of three individual sources oriented in a N-S direction, the highest resolution B-array map may be beginning to distinguish them, giving an appearance of being resolved. In the D and E arrays, the sharp maser “peak” extends  $\sim 7.5 \text{ Jy beam}^{-1}$  above the extended emission, in agreement with the flux density in the B-array spectrum.

A small amount of HCO<sup>+</sup> absorption is visible in the E-array map; however, it is not apparent that the maser linewidth is affected by self-absorption. In this map, the shortest baselines will sample large enough size scales to include the western extension of the continuum that peaks with DR21(OH)-MM2. Furthermore, the HCO<sup>+</sup> emission includes two velocity components associated with extended gas, one at  $-4.7 \text{ km s}^{-1}$ , and another peaking at  $\sim 0 \text{ km s}^{-1}$ . The peak positions of these two velocity components correspond to the continuum peaks of MM1 and MM2 respectively. The high velocity wing of the  $-4.7 \text{ km s}^{-1}$  component is affected by absorption by the continuum in the E-array map, however, the  $0 \text{ km s}^{-1}$  component is not. The D and C array maps with smaller beam sizes (longer baselines) are not affected by this continuum contamination or the extended HCO<sup>+</sup> emission which is resolved out.

Zapata et al. (2012) performed 1mm observations of several

spectral lines around DR21(OH). Included with these observations are CO(2-1) observations which trace an outflow from DR21(OH)-MM2. This outflow appears to be in the plane of the sky (Fig. 3). From this figure, we can see that both the methanol maser and our HCO<sup>+</sup> object appear along the edge of the outflow. This region would be highly shocked, and the energy released from this interaction has the potential to power the maser.

Goldsmith (1972) analyzed the  $J = 1 - 0$  transition of CO and determined that a large range of rotational excitation temperatures, including population inversion, can be produced through collisional excitation in the range of kinetic temperatures and densities found in molecular clouds. It was also concluded that other linear molecules with simple rotational structure, such as HCO<sup>+</sup>, would have the same result. Using the RADEX radiative transfer package (Van der Tak et al. 2007), we performed a test calculation that showed that for collisional interaction such as is suggested here in DR21(OH), it is possible to achieve population inversion in the HCO<sup>+</sup>  $J = 1 - 0$  transition with gas densities of  $\sim 5 \times 10^5 \text{ cm}^{-3}$  and kinetic temperatures  $\sim 50 \text{ K}$  (consistent with kinetic temperatures in outflow shocked regions). This result further supports the conclusion that this HCO<sup>+</sup> is a maser.

#### 4. CONCLUSION

Observations of DR21(OH) have revealed the presence of a compact object which is dominated by non-thermal emission. The extremely compact size of this object coupled with its large brightness leads to the following conclusions:

- The source is co-located with a known strong methanol maser.
- It lies along the edge of an outflow which gives support to previous theories that masers can arise due to the interactions of high velocity outflows with cold, dense clumps of molecular gas.
- Its small spatial size most likely prevented its detection

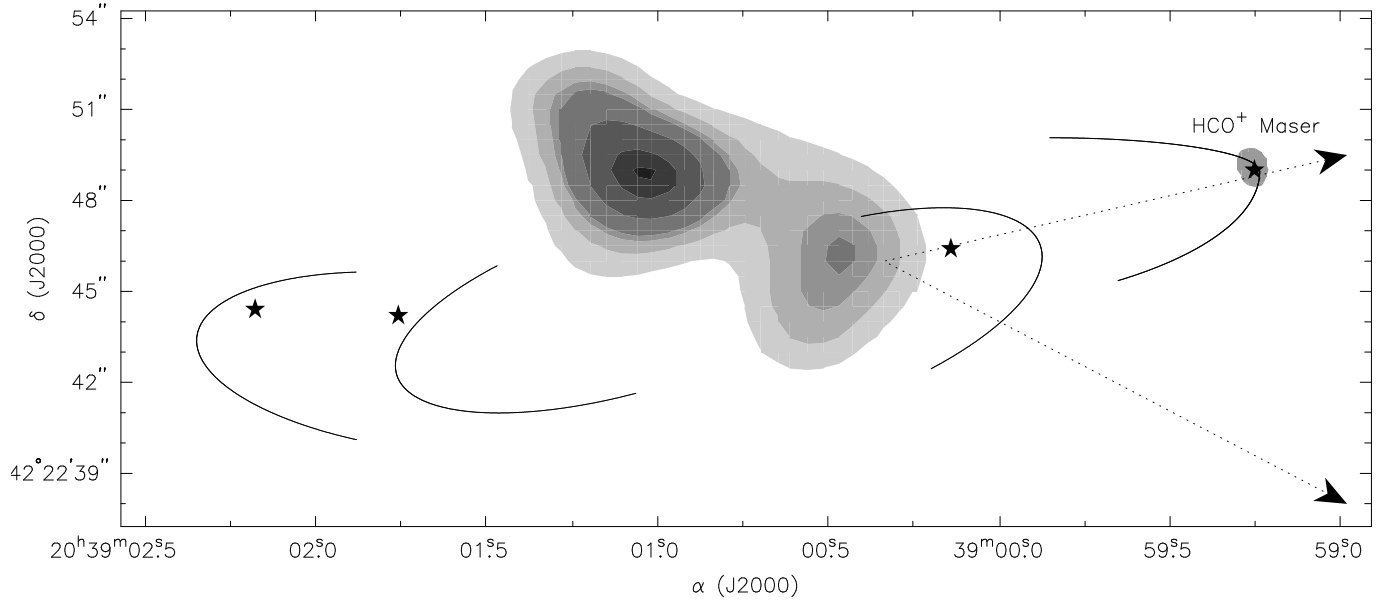


**Figure 3.** Diagram of the position of the  $\text{HCO}^+$  maser with respect to other features of DR21(OH). The shaded contours are of the 112 GHz continuum of DR21(OH). The dotted arrows represent the CO outflow as observed by Zapata et al. (2012). The shaded oval represents the extent of the  $\text{HCO}^+$  object as reported in this paper. The stars represent the positions of methanol masers from Plambeck & Menten (1990). The black curves represent the two sets of bow shocks determined by the loci of 44 GHz methanol masers from Araya et al. (2009). The positions of the masers along the edge of the outflow give strong support to the theory that shocked interactions between outflows and small, high density clumps of molecular gas give rise to these objects. The contour levels of the continuum emission are 0.3, 0.4, 0.49, 0.54, 0.7, 0.9, and 0.99 times the peak flux density of  $0.103 \text{ Jy beam}^{-1}$  in order to show the peaks of both continuum sources.

before now; emission from this source would be beam diluted to levels indistinguishable from thermal emission.

- This object is very likely an unsaturated maser, the first observed in  $\text{HCO}^+$ .

In order to further confirm that this source is indeed a maser, future observations to look for anomalous level populations in higher order  $\text{HCO}^+$  transitions should be performed.

#### 5. ACKNOWLEDGMENTS

Support for CARMA construction was derived from the states of California, Illinois, and Maryland, the James S. McDonnell Foundation, the Gordon and Betty Moore Foundation, the Kenneth T. and Eileen L. Norris Foundation, the University of Chicago, the Associates of the California Institute of Technology, and the National Science Foundation. Ongoing CARMA development and operations are supported by the National Science Foundation under a cooperative agreement (NSF AST 08-38226), and by the CARMA partner universities.

#### REFERENCES

- Araya, E.D., Kurtz, S., Hofner, P., Linz, H., 2009, *ApJ*, 698, 1321  
 Batrla, W., and Menten, K.M., 1988, *ApJ*, 329, 117  
 Bock, D.C.-J., Bolatto, A.D., Hawkins, D.W., Kemball, A.J., Lamb, J.W., Plambeck, R.L., Pound, M.W., Scott, S.L., Woody, D.P., & Wright, M.C.H., "First results from CARMA: the combined array for research in millimeter-wave astronomy", 2006, *Proc. SPIE*, 6267, 13  
 Crutcher, R.M., 1999, *ApJ*, 520, 706  
 Falgarone, E., Troland, T. H., Crutcher, R. M., Paubert, G., 2008, *A&A*, 487, 247  
 Fish, V.L., Muehlbrad, T.C., Sjouerman, L.O., Strelitski, V., Pihlström, Y.M., Bourke, T.L., 2011, *ApJ*, 729, 14  
 Goldsmith, P., 1972, *ApJ*, 176, 597  
 Hakobian, N.S., and Crutcher, R.M., 2011, *ApJ*, 733, 6  
 Padin, S., Sargent, A.I., Mundy, L.G., Scoville, N.Z., Woody, D.P., Leighton, R.B., Masson, C.R., Scott, S.L., Seling, T.V., Stapelfeldt, K.R., Terebey, S., 1989, *ApJ*, 337, 45  
 Plambeck, R.L., and Menten, K.M., 1990, *ApJ*, 364, 555  
 Reid, M.J., and Moran, J.M., 1988, "Galactic and Extragalactic Radio Astronomy", Editors: Verschuur, G.L., and Kellerman, K.I., p. 255-293  
 Slysh, V.I., Kalenskii, S.V., Val'ts, I.E., Golubev, V.V., 1997, *ApJ*, 478, 37  
 Van der Tak, F.F.S., Black, J.H., Schöier, F.L., Jansen, D.J., van Dishoeck, E.F., 2007, *A&A*, 467, 627  
 Zapata, L.A., Loinard, L., Su, Y.-N., Rodriguez, L.F., Menten, K.M., Patel, N., Galvan-Madrid, R., 2012, *ApJ*, 744, 86